GTEM Cell Experimental Set up for In Vitro Dosimetry

Giovanna Calò, Francesco Lattarulo, Vincenzo Petruzzelli

Original scientific paper

Abstract: **A GTEM cell, suitable for assessing possible biological effects induced on cell samples by electromagnetic fields at the typical frequencies of GSM mobile phones, has been designed and set up. Basic environmental requirements for in-vitro biological experiments, involving a GTEM cell, have been assessed by controlling the electromagnetic field distribution and survival conditions. The GTEM cell has been characterized by Standing Wave Ratio (SWR) and Time Domain Reflectometry (TDR) measurements. The impedance matching at the terminal load section has been optimized by considering different hybrid-load configurations. Moreover, optimal exposure conditions for the biological sample have been experimentally evaluated by paying special attention to the E-field scenario inside the GTEM cell at 900 MHz and 1800 MHz frequencies. At last, an experimental evaluation of the Specific Absorption Rate (SAR) is reported.**

Index terms**: Dosmetry, Specific Absorption Rate, GTEM cell.**

I. INTRODUCTION

The wide spread of electromagnetic (e.m.) field sources (i.e. GSM Base Transceiver Stations or broadcast antennas) is responsible for public concern since potential risks for human beings exposed to e.m. fields are not completely understood and satisfactorily assessed. Therefore, even though large amounts of research results have been published, the investigation into possible biological effects of EM fields is still encouraged by national and international health organizations.

Comprehensive information can be provided by in vivo and in vitro dosimetric experiments. Specifically, the in vitro approach, involving biological samples composed by human cell aggregates or tissues, restricts the investigation on the interaction mechanisms between e.m. waves and can, somehow, promote understanding of possible pathologies or behavioral alterations detected by in vivo experiments on laboratory animals.

In spite of the considerable amount of published epidemiological data, ultimately aimed at achieving a correlation between mobile-phone usage and brain cancer, the selection of the electromagnetic field surrogates, directly involved in possible biological effects, still remains an open problem. The number of in vitro investigations performed to sustain cancer promotion models is considerable, too. These studies investigate the changes of the cell surface and of the cell membrane transport of calcium ions, disruption of cell communication, modulation of cell growth, activation of specific gene sequences by modulated ribonucleic acid transcription [1-4]. However, in many cases, e.m. field studies suffer from inconsistencies among different laboratories, owing to the often raised inability in rigorously replicating the experimental conditions. Additionally, the multidisciplinary character of bio-electromagnetism makes the design of in vitro laboratory arrangements and the consequent evaluation, interpretation and correlation of biological data with the observed physical mechanisms a rather crucial task.

Investigations into possible biological effects of e.m. fields require that the exposure system is appropriately designed and the experimental protocol suitably specified. Typical involved parameters are: e.m. field frequency and strength, exposure time and amount of electromagnetic power, expressed in terms of SAR, which has been absorbed by the irradiated sample. Therefore, a number of constraints are to be taken into account and a full characterization of the internal e.m. field and the thermodynamic control of the exposure environment are recommended for a suitable and repeatable design of the dosimetric set up. Moreover, the frequency and the waveform of the excitation signal, the sizes of the exposure device and the environmental conditions should be properly defined by paying special attention to the characteristics of the irradiated object and to the biological effects under investigation. Different exposure set ups and radiation devices, specifically Wire Patch Cells [5], TEM cells and waveguide devices [6] have been proposed for both in vivo [7, 8] and in vitro investigations.

In this paper, a novel GHz Transverse Electromagnetic (GTEM) cell, appropriately designed for in vitro dosimetry, is proposed. The conventional version of the GTEM cell is a valid exposure system for electromagnetic conformity tests on electric and electronic apparatuses [9]. GTEM cell systems have been successfully used for dosimetric experiments and optimal environmental conditions for the exposed sample have been ensured by simultaneously controlling air circulation and temperature [10, 11].

Portability, electromagnetic field uniformity, and shielding are important additional advantages which can be especially appreciated in consideration of the need of attaining a good compromise between the test and total volumes, as well as

Manuscript received December 2, 2005 and revised September 5, 2006.

Giovanna Calò, Francesco Lattarulo, and Vincenzo Petruzzelli are with the Dipartimento di Elettrotecnica ed Elettronica, Politecnico di Bari, Italy (e-mail: petruzzelli@poliba.it).

the support of the only fundamental TEM mode up to frequencies of a few GHz.

II. GTEM Cell for In Vitro Dosimetry

The GTEM cell is a tapered coaxial waveguide commonly used in Electromagnetic Compatibility (EMC) tests to simulate the free-space radiation conditions in a shielded, thus restricted, environment. Since accurate and repeatable measurements can be performed for operating frequencies up to a few tens of GHz, the GTEM cell turns out to be a valid alternative to the TEM cell, the latter being largely used at lower frequencies. Additionally, a uniform e.m. field distribution can be attained in the test core of the shielded overall volume. The shielding system prevents inwardly directed disturbances from affecting the inner e.m. field. Simultaneously, the GTEM cell is designed to meet the EMC requirements for outside instrumentation, control circuitry and operator safety.

A. GTEM Cell Design

On the basis of the aforesaid electromagnetic characteristics, the GTEM cell seems feasible for dosimetric experiments. However, a GTEM cell requires to be properly designed for in vitro experiments by taking into account the geometrical and environmental constraints. Specifically, the cell must be introduced into a commercially available incubator, a prerequisite for the biological sample survival. In the present case, the incubator has sizes 50 cm x 50 cm x 70 cm. Internal humidity and temperature conditioning and dosimetric parameter control are additional requirements to be taken into account. Everything considered, the maximum size of the proposed GTEM cell has been set equal to L=45 cm, whereas the air flow has been permitted by ad hoc small apertures made on the GTEM cell walls. The apertures have been carefully designed to ensure abatement of e.m. field interfering with the incubator control circuitry.

Electromagnetic field uniformity is a basic prerequisite for making the dosimetric tests reproducible and it can be reached if resonance phenomena and reflections in the GTEM cell are prevented. This imposes that the impedance matching condition must be satisfied both along the propagation direction and at the terminal section by an appropriate design of the GTEM cell as regards the size and the adopted absorbing load.

A GTEM cell can actually be considered as a tapered stripline with an offset inner conductor, here referred to as septum, which allows the propagation of the TEM mode. Such a waveguide behaves as a transmission line with an associated characteristic impedance depending on the geometrical parameters of the structure. Thus, in order to achieve a 50-Ω characteristic impedance and to maximise the test volume, the relevant geometrical parameters of the GTEM cell transverse section, shown in Fig.1, were chosen by using the following expression:

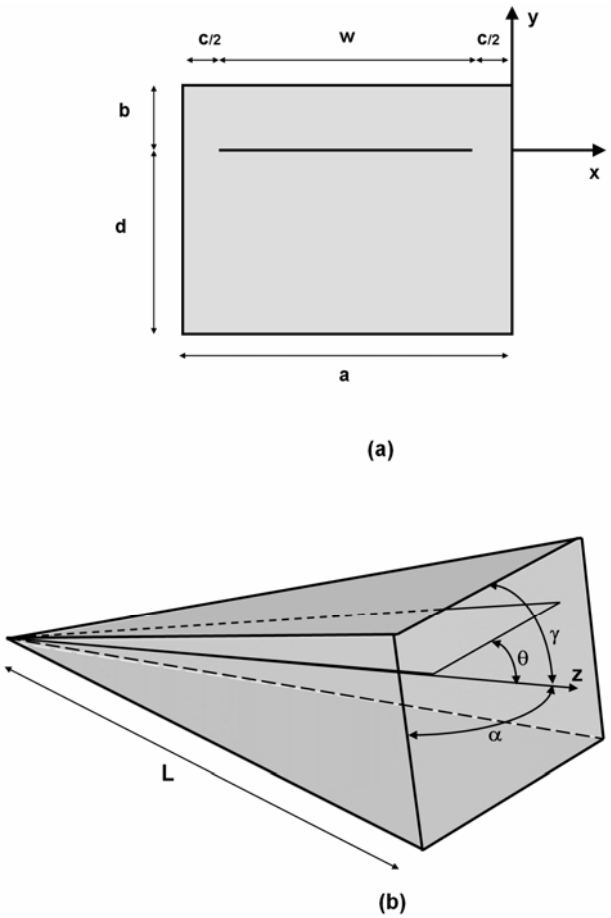

Fig. 1. GTEM cell scheme: a) cross section; b) perspective.

$$\frac{Z_0}{\eta} = \frac{\varepsilon\,\varepsilon_0}{C} \tag{1}$$

where Z_0 is the assigned cross-sectional characteristic impedance, η is the free-space characteristic impedance and ε is the relative permittivity of the medium. The capacitance C and, in turn, the characteristic impedance of the equivalent stripline can be expressed as an implicit function of the geometrical parameters as follows [12]

$$C = 2\varepsilon_0\varepsilon \left\{ \frac{\left[1+\left(1-\chi^2\right)A_1\right]K - A_1\left[\left(1+\xi\right)^2-\chi^2\right]E}{\left[1-\xi\left(2+\xi\right)A_1\right]K' + A_1\left[\left(1+\xi\right)^2-\chi^2\right]E'} \right\} \text{mod}\,\kappa. \tag{2}$$

In (2),

$$\begin{cases} \chi = \dfrac{1}{2}\left(\cos\phi_1 + \cos\phi_2\right) \\ \xi = \dfrac{1}{2}\left(\cos\phi_1 - \cos\phi_2\right), \\ \kappa = \dfrac{2\sqrt{\xi}}{\left[\left(1+\xi\right)^2-\chi^2\right]^{1/2}} \end{cases} \tag{3}$$

$$A_1 = \left[\frac{\cosh\left(\frac{\pi(b+d)}{a}\right) - \cosh\left(\frac{\pi(d-b)}{a}\right)}{\sinh\left(\frac{\pi(b+d)}{a}\right)} - 1 \right],$$

and

$$\begin{cases} \phi_1 = \frac{\pi}{2a}(a-w) \\ \phi_2 = \frac{\pi}{2a}(a+w) \end{cases}.$$

Equations (2) and (3) show the dependence of the capacitance C on the geometrical parameters, a, b, d, and w of Fig.1, expressed as a function of A_1, ϕ_1 and ϕ_2. In addition, K = K(κ) and E = E(κ) represent the complete elliptic integral of the first and of the second kind, respectively, κ being defined in (3) and K' = K(κ') and E' = E(κ') denote the corresponding integrals calculated for $\kappa' = \left[1-\kappa^2\right]^{1/2}$.

Resolving the above equations for the GTEM cell geometrical sizes and imposing relative maximization of the inner test volume, ultimately leads to an aspect ratio (b+d)/a=2/3 and to asymmetrical location of the internal septum at height d=3(b+d)/4. The geometrical parameters were calculated by using the following additional formulas

$$\begin{cases} a = 2\ L\ \tan(\alpha) \\ b = L\left[\tan(\gamma) - \tan(\theta)\right] \\ d = L\left[\tan(\gamma) + \tan(\theta)\right] \end{cases} \quad (4)$$

In (4), α = π/12, γ = π/18, θ = π/36 are the GTEM-cell aperture angles, shown in Fig.1 (b), whereas L = 45 cm is the permissible maximum length of the GTEM cell. The choice of L is substantially dictated by the need of locating the GTEM cell into the incubator.

Once the above geometrical parameters have been identified, the characteristic impedance Z_0/η, normalized to the vacuum characteristic impedance, can be calculated by (1) as a function of the septum width to cell width ratio w/a. Fig.2 shows the curve useful for the GTEM cell design and the dashed lines correspond to the required 50-Ω characteristic impedance.

In synthesis, according to (1), the optimized geometrical sizes are: cell length L=45 cm, aspect ratio (b+d)/a=2/3, septum width to cell width ratio w/a = 0.7. Moreover, the tapered shape of the GTEM cell allows the same aspect ratio to hold throughout the propagation direction, thus ensuring a constant characteristic impedance. In particular, a = 24 cm, b = 4 cm and d = 12 cm have been chosen for the terminal section. Furthermore, in order to obtain a uniform E-field distribution in the test region, suitable absorbing materials were adopted to avoid wave reflections at the terminal load section.

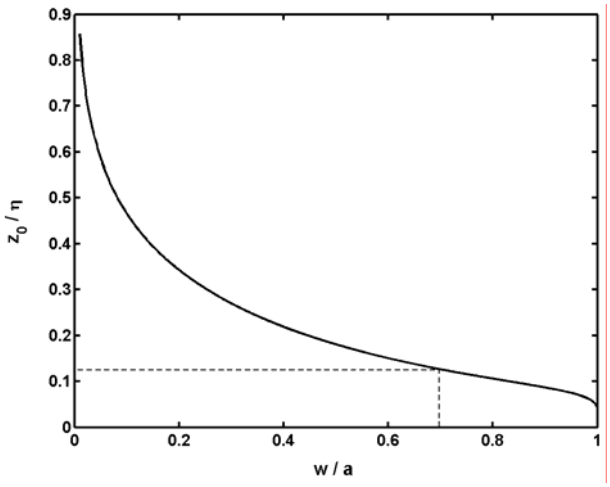

Fig. 2. Characteristic impedance Z_0 normalized to the vacuum characteristic impedance η as a function of the septum to GTEM-cell width ratio w/a.

B. Electromagnetic Analysis

The expected E-field pattern in the GTEM-cell cross section has been calculated by means of a home-made computer code based on the Transverse Resonance Diffraction (TRD) method [13]. By applying the TRD method, the complete electromagnetic analysis of the GTEM cell was performed. In fact, the TEM-mode pattern, the higher-order mode cutoff frequencies and the corresponding e.m. field distribution were simulated by expressing the propagating mode components in terms of auxiliary scalar potentials $\Pi_k(x,y)$. Accordingly, the auxiliary scalar potentials

$$\Pi_k(x,y) = \sum_{n=0}^{N} \Pi_{kn}(x,y)$$

have been defined by a series expansion involving N functions $\Pi_{kn}(x,y)$. Each of them satisfies the boundary conditions in the cross-section of the GTEM cell, shown in Fig.1 (a). Thus, for the TE modes, the following set of equations

$$\begin{cases} \Pi_k(x,y) = \sum_n \frac{2V_n\delta_n}{\sqrt{a}} \cos\left(\frac{n\pi x}{a}\right) \frac{-\cos\left[k_n(y-b)\right]}{\sin(k_n b)}, \\ \qquad\qquad 0 \le y \le b \\ \Pi_k(x,y) = \sum_n \frac{2V_n\delta_n}{\sqrt{a}} \cos\left(\frac{n\pi x}{a}\right) \frac{\cos\left[k_n(y+d)\right]}{\sin(k_n d)}, \\ \qquad\qquad -d \le y \le 0 \end{cases} \quad (5)$$

has been obtained. The parameters of (5) are:

$$\begin{cases} \delta_n = 1/\sqrt{2}, & n \neq 0 \\ \delta_n = 1/2, & n = 0 \end{cases}$$

and

$$\begin{cases} k_n^2 = k_{tk}^2 - (n\pi/a)^2 \\ k_{tk}^2 = k_0^2 - \beta_k^2 \end{cases}, \quad (6)$$

where k_{tk} is the cut-off wavenumber of the k-th mode and β_k is the phase constant, whereas the n-th V_n value in (5) identifies the normalization coefficient for the function $\Pi_{kn}(x,y)$ [12].

The transversal ($\mathbf{h}_{tk}$ and $\mathbf{e}_{tk}$) and longitudinal ($\mathbf{h}_{zk}$) components of TE mode assume the following expression:

$$\begin{cases} \mathbf{h}_{tk}(x,y) = h_{xk}(x,y)\mathbf{a}_x + h_{yk}(x,y)\mathbf{a}_y = -\dfrac{\nabla_t \Pi_k(x,y)}{k_{tk}} \\ \mathbf{h}_{zk}(x,y) = \dfrac{k_{tk}\Pi_k(x,y)}{j\omega\mu}\mathbf{a}_z \\ \mathbf{e}_{tk}(x,y) = e_{xk}(x,y)\mathbf{a}_x + e_{yk}(x,y)\mathbf{a}_y = -\dfrac{\nabla_t \Pi_k(x,y)\times\mathbf{a}_z}{k_{tk}} \end{cases} \quad (7)$$

Similar formulas can be obtained for the TM modes, whereas the electromagnetic field pattern of the fundamental TEM mode is calculated from the general TE mode formula by setting the cutoff frequency equal to zero.

Fig.3 shows the E-field curves of the fundamental TEM mode calculated in the transversal section at distance z = 23 cm from the source input port. It is worth observing that, in the region under the septum (y < - 0.02 m), the E-field assumes an almost uniform pattern along the propagation direction z. Indeed, responsible for a possible perturbation of the e.m. field distribution and uniformity is the activation of higher-order modes. However, the tapered shape of the GTEM cell yields some higher-order modes to be originated only in correspondence of the larger sections. In fact, the "essential" modes are related to the geometrical size of the GTEM cell transverse section. Nevertheless, further modes can be excited either by cross-sectional discontinuities or by the presence of the biological sample which introduces dielectric inhomogeneity along the propagation direction [14]. Indeed, the "non-essential" modes, excited by such discontinuities, are verified to hold negligible. However, the contribution of "essential" higher-order modes to the total e.m. field can be minimized by appropriately positioning the biological sample. In fact, owing to power exchange with the TEM mode described by the generalized telegrapher equations [13], the amplitude of higher-order modes increases with the distance from the section in which they are excited.

Therefore, the optimal position of the biological sample can be chosen in order to reduce the number of propagating modes and the induced e.m. field perturbation. For this purpose, the transverse resonance condition has been applied to the field components of (7) and the corresponding eigenvalue equation has been solved to calculate the cutoff frequencies of the TE and TM higher-order modes.

The propagation constants β_k of the higher-order modes have been calculated, as a function of the propagation direction z and of the operating frequency f, via the formula:

$$\beta_k = k_0\sqrt{1-\left(\frac{z_L f_{ck}}{z\, f}\right)^2} \quad (8)$$

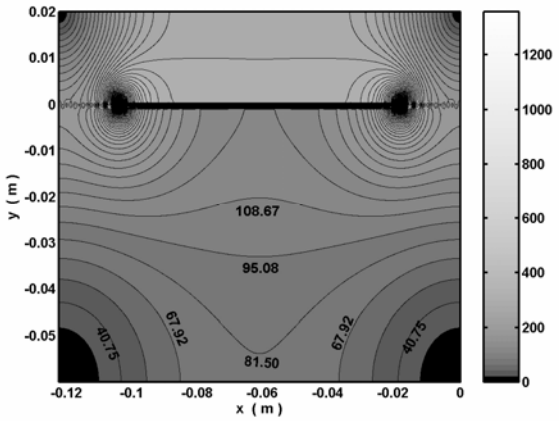

Fig. 3. Contour lines of the electric field magnitude calculated in correspondence of the GTEM-cell cross section z= 23 cm.

where, k_0 is the vacuum wavenumber and f_{ck} is the cutoff frequency of the k-th mode, calculated by the TRD method in correspondence of the terminal section z_L.

Fig. 4 illustrates the behavior of the normalized phase constants β_k/k_0 of the TE (solid lines) and TM (dashed lines) modes at the frequencies f = 0.9 GHz (Fig.4 (a)) and f=1.8 GHz (Fig. 4 (b)), respectively, as a function of the longitudinal direction z for the 0.450-m long GTEM cell under examination. On the one hand, Fig. 4 (a) highlights that the monomodality at f=0.9 GHz is ensured from z = 0 m to z = 0.30 m, namely where the first TE_1 higher-order mode starts to propagate. On the other hand, Fig.4 (b) shows that for f=1.8 GHz, the only fundamental TEM mode propagates along the GTEM cell structure for z < 0.150 m. Therefore, the sample under test should be placed in this region at z < 0.150 m to exploit the irradiation of the only TEM mode during the experiments carried out at f = 1.8 GHz.

A further constraint for the sample location, linked to the assumed field uniformity, imposes that the maximum size of the sample under test must not exceed one third of the distance between the septum and the outer conductor of the GTEM cell [14]. On the basis of such constraint, the optimal position of the biological sample is at z = 0.23 cm. Therefore, at f = 900 MHz, the biological sample is irradiated only by the TEM mode, whereas, as the frequency attains 1800 MHz, the same sample is irradiated also by the first TE mode. Fortunately, this occurence negligibly influences the incident E-field pattern owing to the much lower electromagnetic power associated to the higher-order modes with respect to that carried by the dominant TEM one. Of course, the amplitude of higher-order modes increases as a function of the propagation direction, owing to the power exchange with the TEM mode. In fact, the power transfer between the TEM wave and the higher-order modes is more effective as the relevant propagation constants β_k approach k_0 (see Fig.4). Nevertheless, from the generalized telegrapher equations [13], we calculate that, at the section z = 0.230 m from the GTEM cell apex, the overall power is almost completely associated to the TEM mode (about 95 %) for f = 1.8 GHz, whereas only a

small amount of power (about 5 %) is associated to the first higher-order mode TE_1.

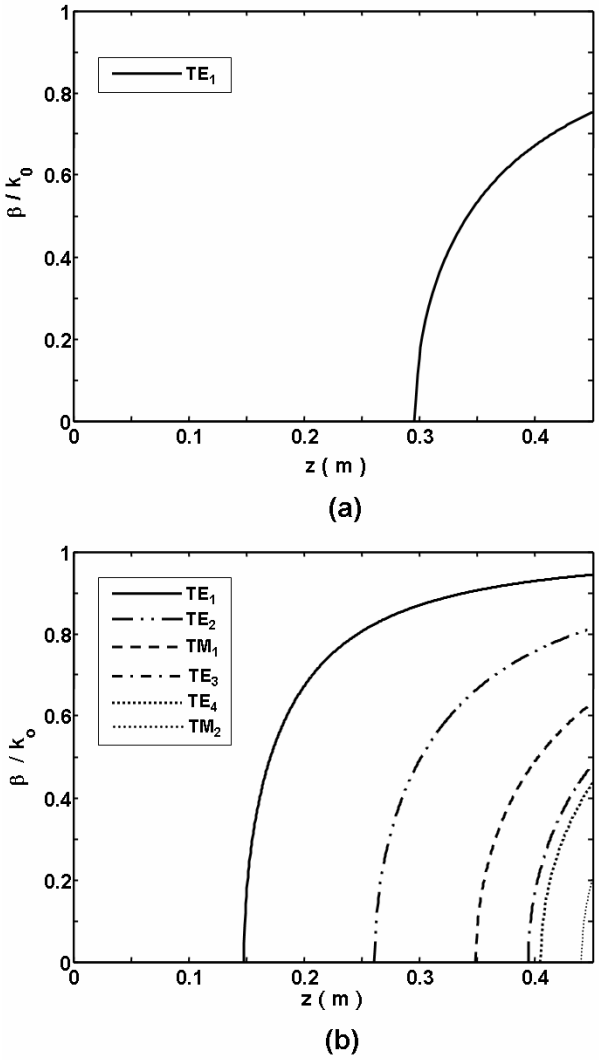

Fig. 4. Normalized phase constants β/k_0, associated to the first TE (solid lines) and TM (dashed lines) modes propagating along the longitudinal direction at the frequency: a) f = 0.9 GHz, b) f = 1.8 GHz as a function of z.

III. EXPOSURE SYSTEM

According to the abovementioned design criteria a GTEM cell prototype has been realized (see the photo of Fig.5). Owing to the high humidity rate of the incubator environment, the GTEM cell walls have been made of oxidation-free aluminum panels. The air flux in the GTEM cell has been permitted by the presence of small apertures on the side walls. As Fig.5 shows, a further waveguide aperture under cutoff condition has been realized on the side door, to allow the control probes to be crossed during the exposure. The GTEM cell septum is made by a printed circuit board (PCB) with an inserted 50-Ω impedance network connecting the inner conductor to the terminal GTEM-cell wall. The 50-Ω resistive load is needed for the terminal load matching at the lowest frequency range (from zero up to a few kHz). For higher frequencies, suitable absorbing materials, compatible with the small size of the GTEM cell, have been used to prevent reflections.

The GTEM cell experimental equipment is depicted in Fig. 6. The exposure system is linked, via an SMA connector, to the amplifier and to the signal generator; the 50-Ω impedance matching allows the maximization of the power transfer to the device. A personal computer controls the signal generator via a GPIB interface in order to establish suitable electromagnetic exposure conditions for different values of the operating frequency and of the SAR. The input power and the duration of the exposure cycles, together with power-on and power-off intervals, can also be assigned.

Fig. 5. Photo of the GTEM cell prototype located in the incubator.

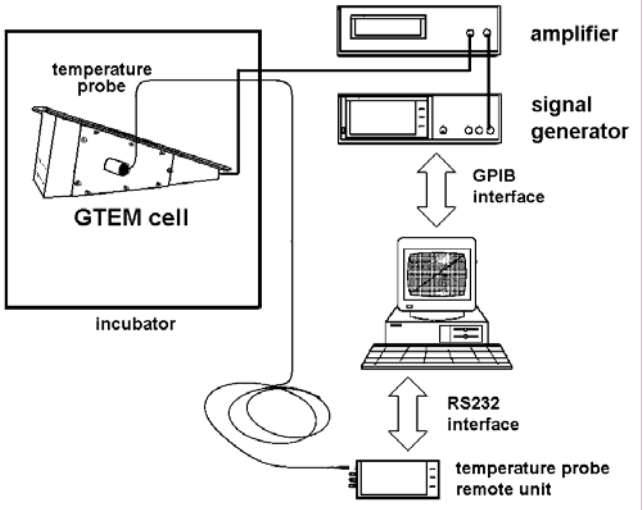

Fig. 6. GTEM cell experimental set up.

A set of control probes (i.e. fibre-optic temperature probes and miniaturized optical E-field probes) can be simultaneously inserted into the GTEM cell during the exposure for monitoring the experimental conditions with no significant perturbation of the e.m. irradiation. As an example, Fig.6 shows a temperature fiber-optic probe connected, through the GTEM cell side door aperture, to its remote unit by a fiber optic cable. In this case, the temperature is monitored by the computer via RS232.

IV. GTEM CELL CHARACTERIZATION

The electromagnetic characterization of the GTEM cell prototype is a prerequisite for establishing the exposure conditions during the actual dosimetric experiments. Therefore, a complete knowledge of the GTEM cell features allows the input signal to be related to the SAR of the biological sample and, then, possible biological effects to be assessed.

A. Terminal load optimization

In order to achieve the electromagnetic field uniformity in the test volume, the impedance matching condition has primarily been verified. In particular, optimization of the impedance matching along the propagation direction and at the terminal load section has been carried out by the Standing Wave Ratio (SWR) and the Time Domain Reflectometry (TDR) measurements.

The TDR measurement has shown an almost constant 50-Ω characteristic impedance along the propagation direction, whereas a maximum value of the impedance mismatch (50±10 Ω) has been calculated in correspondence of the input section, where a noticeable transition from the coaxial SMA connector to the septum occurs. In this way, a slight reduction of the power transfer efficiency at the input section is induced. A further negligible change of the characteristic impedance is also present in correspondence of the side door of the GTEM cell, due to the small change in the transverse section size.

Owing to the reduced sizes of the proposed GTEM cell, the impedance matching at the terminal load section requires an accurate analysis. Actually, to maximize the available test volume, the length of the absorbing materials should be less than 15 cm. Therefore, in spite of their broadband matching capability, long pyramidal absorbers were deliberately ignored for the GTEM cell under examination, whereas alternative solutions were examined.

Aiming at analyzing and comparing the frequency behavior of different load configurations, the GTEM-cell SWR has been characterized in the frequency range from 0.13 GHz to 4 GHz for three different absorbing materials. In particular, Fig.7 shows the SWR measured for the resistive network load together with: 1) commercially available short pyramidal dielectric absorbers (dotted curve) made by 5-cm pyramids mounted on a 2-cm base; 2) nickel-zinc ferrite tiles (solid curve); 3) 3-cm thick brick-shaped absorbers having the size

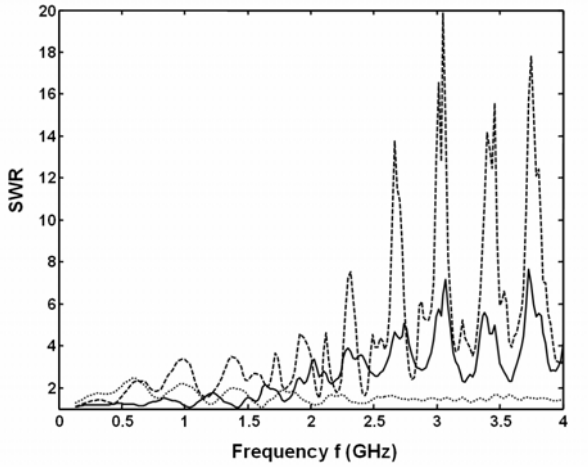

Fig.7: SWR vs. frequency for resistive network load with pyramidal dielectric absorbers (dotted curve), ferrite tiles (solid curve), and graphite absorbers (dashed curve).

of the GTEM cell terminal cross-section, here referred to as graphite absorbers, home-made by enriching dielectric foam with graphite powder (dashed curve).

As expected, the pyramidal dielectric absorbers showed a high SWR, with peak value equal to SWR=2.5, in the lower frequency range up to 1 GHz. On the other hand, the SWR decreased by increasing the frequency, assuming a maximum value SWR = 2 in the range from 1 GHz to 2 GHz. Incidentally, the best performances (SWR=1.6) was achieved in the range from 2 GHz to 4 GHz, where the pyramidal absorbers became rather elongated with respect to the wavelength.

Conversely, an opposite behavior with respect to the frequency was experienced for nickel-zinc ferrite tiles and graphite absorbers, both showing resonance peaks (SWR>5) for frequencies higher than 2 GHz, whereas lower SWR values were obtained in the range up to 2 GHz. However, in the range up to 2 GHz, the improvement of the matching capability reached a minimum for the graphite absorbers since the corresponding SWR assumed a peak value equal to about SWR = 3.5. On the contrary, the ferrite tiles were more effective, particularly, in the lower frequency range (up to 0.6 GHz) where SWR < 1.4, whereas a peak value SWR = 2.2 degraded the matching condition around the 1800 MHz frequency.

On the basis of the aforesaid measurements, none of the considered absorbing materials appeared suitable for meeting the impedance matching condition and effectively reducing resonances in the region around the two f=900 MHz and f=1800 MHz frequencies.

Hybrid load configurations, obtained by the combination of these materials, allowed their different frequency behavior to be exploited. For this purpose, three further configurations of the terminal load were tested by measuring the SWR in a more restricted frequency range, namely from 0.5 GHz to 2 GHz. Fig. 8 shows the SWR measured for three different loads: i) resistive network load (solid curve); ii) resistive network load together with a combination of ferrite tiles and

graphite absorbers (dashed curve); iii) resistive network load together with a combination of ferrite tiles and pyramidal dielectric absorbers (dotted curve). The results have been compared with those obtained by using the resistive network load i) that represents the worst-case of impedance matching (assuming interesting performance only for frequencies lower than a few kHz).

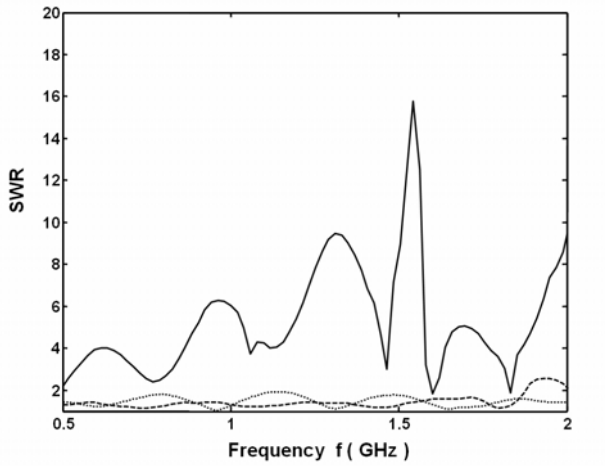

Fig. 8. SWR vs. frequency: i) resistive network load (solid curve); ii) resistive network load together with graphite absorbers and ferrite tiles (dashed curve); iii) resistive network load together with pyramidal dielectric absorbers and ferrite tiles (dotted curve).

Fig. 8 shows a strong resonance, corresponding to the only resistive network load (solid curve): this resonance can be effectively reduced using either ii) or iii) hybrid load configurations. These load configurations assure SWR values lower than 1.9, substantially in the whole frequency range from f = 0.5 GHz to f = 2 GHz. In particular, for the hybrid load configuration ii), SWR = 1.39 and SWR=1.15 were measured at the frequencies f = 0.9 GHz and f=1.8 GHz, respectively. On the other hand, SWR = 1.36 at f = 0.9 GHz and SWR = 1.45 at f=1.8 GHz were obtained for the load configuration iii). Hence, both the two hybrid load configurations resulted feasible for the GTEM cell, both achieving a good compromise between low SWR and overall space occupied.

A further investigation on the terminal load performance was carried out by measuring the internal electric field both along the propagation direction and inside the test region, where the biological sample was located, in order to verify the best exposure conditions.

B. Electric Field Measurement

The electric field in the GTEM cell has been measured by using a miniaturized (5.6 mm x 5 mm x 5 mm) optical E-field probe [16] at the f=900 MHz and f=1800 MHz frequencies. This innovative measurement system consists of a probe connected to a spectrum analyzer via fiber optics and of an interposed remote optical/electrical conversion unit. The electrical output-signal is proportional to one spatial component of the measured electric field strength. Therefore, three orthogonally oriented measures have been made to fully evaluate the electromagnetic field. The probe negligibly perturbs the e.m. field inside the GTEM cell owing to the optical technology adopted and its miniaturization in comparison to the test domain.

At first, the three E-field components have been measured in different sections along the propagation direction z and compared with the numerical results of the computer code simulation. The optimal exposure conditions, with particular reference to both the GTEM cell and the termination load performance, have been estimated in terms of deviation from the optimal numerical case.

For this purpose, a numerical computer code (CST MicroWave Studio) based on the Finite Integration Technique (FIT) has been used for simulating the GTEM cell. The calculated E-field assumes optimized values due to the 50-Ω impedance matching condition at the end face of the GTEM-cell.

The E-field components have been measured in the GTEM cell, at the two frequencies f=900 MHz and f=1800 MHz, for both the configurations ii) and iii) of the absorbing terminal load. The measurement has been carried out for a low input power level (P_{in} = 220 mW) compatible with the lineary range of the E-field optical probe (according to the data sheet, 1-dB compression point occurs at about 100 V/m). In particular, the inwardly directed power P_{in} = 220 mW was evaluated at the SMA coaxial connector section by taking into account the output power level of the signal generator, the amplifier gain, and the connecting cable attenuation.

It is worth mentioning that measurements and simulations were carried out for different input power levels. On the one hand, the simulation was performed at input power P_{in}=0.5 W, as typically used in CST simulations. On the other hand, since the measured internal electric field values are required to be within the linearity dynamic range of the optical probe, the experimental characterization of the GTEM cell needed a proper input power (i.e. P_{in}=220 mW). Obviously, for the sake of comparison, the measured and the numerical values were normalized to the same input power. Therefore, the linear dependence of the E-field values on the input-power square root was verified for different measurement points. Hence, the E-field values, corresponding to the assigned input power level (i.e. P_{in}=0.5 W), were predicted from the measurements by simply considering their linear dependence on the square root of the input power.

Figs. 9 (a) and (b) show the E-field strength as a function of the propagation direction z, at the investigated frequencies f = 0.9 GHz and f = 1.8 GHz, respectively, for an input power value P_{in} = 0.5 W. The strength calculated by the CST (solid line) is compared with the measured ones corresponding to the two hybrid load configurations. More precisely, the measured values (dots) and the corresponding polynomial fitting curve (dashed line), are referred to the case of a hybrid load configuration ii) (resistive network load in combination with graphite absorbers and ferrite tiles). Instead, the

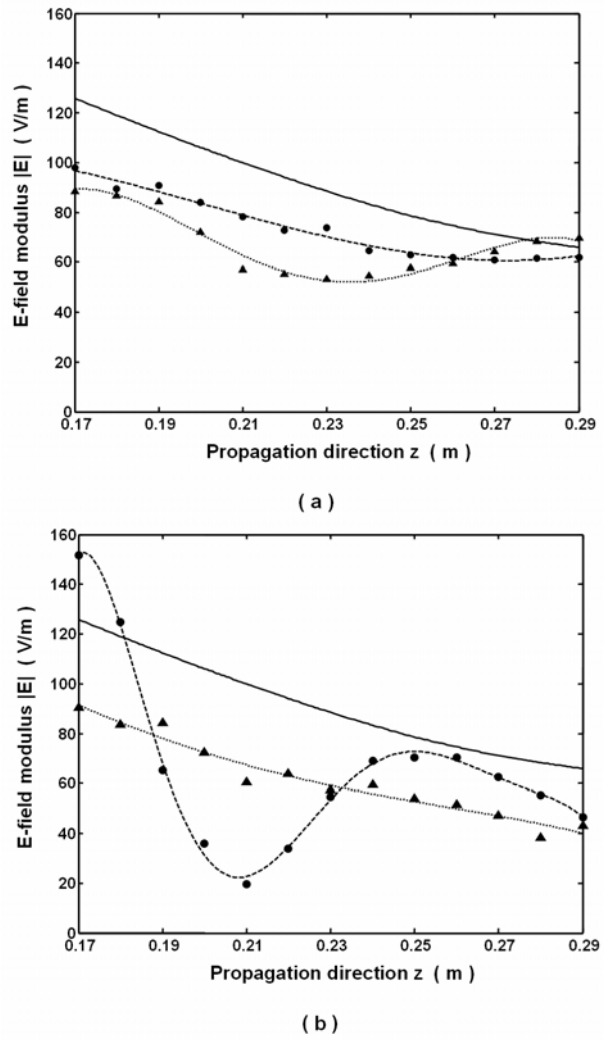

Fig. 9. E-field distribution along the z-axis at f = 0.9 GHz (a) and 1.8 GHz (b) for the simulation (solid curve), for the load configuration ii) (dots for the measurement and dashed curve for the corresponding polynomial fitting), and for load configuration iii) (triangles for the measurement and dotted curve for the corresponding polynomial fitting).

measured values (triangles) and the corresponding polynomial fitting curve (dotted line) are referred to the case of load configuration iii) (resistive network load together with pyramidal dielectric absorbers and ferrite tiles).

As Fig.9 (a) shows, at the frequency f = 0.9 GHz, a good agreement between simulated and measured E-field values occurs for the load configuration ii) (dots and dashed curve), whereas a slightly resonant behavior appears in the case of load configuration iii) (triangles and dotted curve). Therefore, the graphite absorbers and ferrite tiles are appropriate for the frequency f = 0.9 GHz. Conversely, Fig.9 (b) shows a noticeable resonant behavior for the load configuration ii) (dots and dashed curve), whereas a good agreement between simulated and measured E-field values was achieved for the load configuration iii) (triangles and dotted curve). As a result, the pyramidal absorbers and ferrite tiles are appropriate for the frequency f = 1.8 GHz.

Therefore, different configurations of the terminal load are recommended in dependence of the used operating frequency. Other absorbing material configurations are being investigated to find more optimized GTEM cell impedance matching by using load configuration for both the frequencies.

It is worth noticing that, although the optimal load configurations were used for each frequency, the measured E-field values are lower (about 20 %) than the simulated ones. Responsible for such a behavior are both the relatively high impedance mismatch (50±10 Ω) occurring at the input port and the power losses neglected in the numerical simulation. Nevertheless, the optimal curves of Fig. 9, corresponding to load configuration ii) in Fig.9 (a) and iii) in Fig.9 (b), assume almost the same behavior of the simulated curve. Therefore, by virtue of the linear law governing the E-field as function of the square root of the input power, the latter must be increased to compensate the difference between the measured and calculated E-field values.

III. SAR Evaluation

Aiming at evaluating the exposure conditions during dosimetric experiments, a combined technique, involving experimental and numerical electric fields, was used for assessing the SAR of the sample under test. According to the adopted procedure, a comparison between simulated and measured E-field values is the prerequisite for assessing exposure conditions and, consequently, the SAR pertaining to the irradiated biological sample.

Therefore, a full-wave numerical model of the realized GTEM cell was developed by CST. Although the geometry of the GTEM cell prototype has been modeled carefully, a few simplified conditions have been introduced to reduce the model complexity and the linked computation time. More precisely, the SMA connector and its transition to the GTEM cell septum have been neglected. Moreover, a waveguide port was defined, according to CST specifications, by cutting the GTEM cell pyramidal shape at the SMA-connector-to-septum transition. Another waveguide port was similarly defined at the terminal section of the GTEM cell, thus avoiding the supplementary modeling of the absorbing materials. Owing to this choice, a optimal impedance matching condition at both the input/terminal load sections, met by simulated characteristic impedances equal to Z_0=50.17 Ω and 50.73 Ω at the former and the latter waveguide ports, respectively, was achieved. Under the above circumstances, the developed numerical model was assumed to give the more accurate results.

For the purpose of assessing the exposure conditions during the dosimetric experiments, the E-field magnitude was numerically and experimentally evaluated in nine points (see point notations A to I over the dashed contour of Fig. 10). These points surround the section placed at a distance z = 23 cm from the apex of the GTEM-cell pyramidal shape, namely

in the region where the Petri dish will be placed during the experiments.

In particular, the electric field levels were measured for both the optimal configurations of the terminal load. As expected, the best agreement between the simulated and measured values was obtained when graphite and ferrite load ii) and ferrite and dielectric pyramidal absorbers iii) were used for f = 0.9 GHz and f=1.8 GHz, respectively.

The nine values of the measured E-field strength (f = 0.9 GHz and 1.8 GHz; input power P_{in}=0.5 W) are summarized in Table I together with the numerical values.

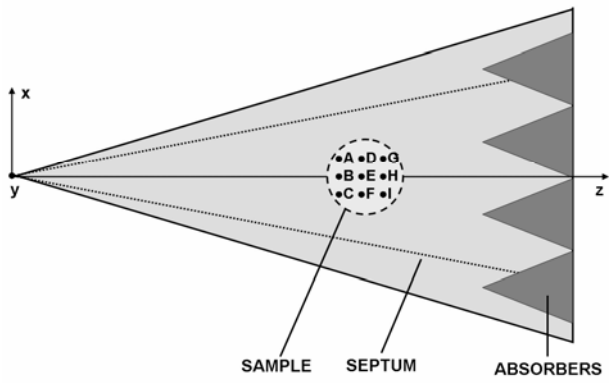

Fig.10: E-field measurement points in the test region surrounding z = 23 cm.

TABLE I
E-FIELD MEASUREMENTS AND CALCULATIONS IN NINE POINTS OF THE TEST VOLUME.

	f=0.9 GHz	f=1.8 GHz	simulated
A	82.92	71.94	96.12
B	86.09	68.53	97.69
C	82.29	67.95	96.12
D	77.75	61.08	90.12
E	82.76	65.24	91.49
F	71.51	57.96	90.12
G	83.65	63.62	84.95
H	84.71	59.47	86.17
I	71.69	60.91	84.95
Mean	80.37	64.07	90.85
Emin/Emax	0.83	0.81	0.87

It is worth noticing that the measured electric field is lower than the simulated one, whereas a good agreement is achieved as regards the E-field uniformity (expressed in terms of E-field minimum to maximum ratio). Moreover, the linear dependence of the electric field magnitude on the input power square root has been verified for each of the nine measurement points. By comparing the experimental and the simulated results, the SAR of the exposed biological sample has been calculated. In fact, owing to the impossibility to measure, with our probe, the E-field inside the biological sample, the linked SAR was calculated by combining the simulated CST results and the E-field measured in the GTEM cell. In particular, the Petri dish, filled with cell medium, was included in the numerical model of the GTEM cell. For this aim, the following parameters were used: Petri dish internal diameter d=5 cm and height h=1.5 cm, real and imaginary components of the cell medium complex permittivity ε' = 77.1, ε'' = 37.9 and ε' = 76.3, ε'' = 23.5 for f = 900 MHz and 1.8 MHz, respectively [17]. In particular, the first-order Debye dispersion model for the dielectric parameters of the cell medium was used in the simulation frequency range (f = 0 - 3 GHz). In addition, a constant relative permittivity ε' = 2.55 was used for the loss-free (ε'' = 0) plastic container of the Petri dish. Moreover, the discretization grid associated to the GTEM cell numerical model was made of 749074 mesh cells, whereas in the region occupied by the biological sample a more refined grid, composed by 10265 mesh cells, was adopted.

The calculated SAR_m, averaged over the sample volume for the input power P_{in}=0.5 W, was found to be equal to 0.079 W/kg at f = 0.9 GHz and 0.638 W/kg at f = 1.8 GHz.

It is worth considering that the numerically predicted exposure conditions (specifically, incident E-field strength and mean SAR) can be achieved during the experiment by moderately increasing the input power P_{in} (i.e. from P_{in}=0.5 W used for the simulated case to P_{in} =0.64 W at f=0.9 GHz and P_{in} =1 W at f=1.8 GHz for the dosimetric experiment).

Therefore, owing to the linear dependence of the E-field on the input power square root, the actual SAR during the exposure experiment was safely reached by assigning the appropriate value of the input power.

IV. CONCLUDING REMARKS

A special version of a GTEM cell exposure set up, recommended for in vitro dosimetric investigations on electromagnetic field (e.g. GSM radio mobile signals) biological effects, has been proposed. Accordingly, the GTEM cell was designed and a prototype was realized by taking into account ad hoc requirements. The exposure set up was defined, too.

A 50-Ω characteristic impedance along the propagation direction was obtained by an optimal choice of geometrical parameters. The GTEM cell exposure conditions were optimized, too by using a Transverse Resonance Diffraction method electromagnetic analysis.

In particular, the Petri dishes were appropriately located in the GTEM region where the electromagnetic field assumes a uniform behavior (z=0.23 m). In this region, the only TEM wave propagates at f=0.9 GHz whereas the first higher-order TE_1 mode propagates at f=1.8 GHz. However, the perturbation induced by the TE_1 higher order mode results negligible because of the much lower power amount involved.

For the purpose of optimizing the impedance matching condition, different configurations of the terminal load were

investigated by the SWR and the TDR measurements. Further useful information on the terminal load performance was obtained by comparing the calculated and the measured values of the E-field strength along the propagation direction. Two different optimal hybrid load configurations were identified for the two operating frequencies: resistive network load combined to graphite absorbers and ferrite tiles for f = 0.9 GHz and resistive network load combined to pyramidal dielectric absorbers and ferrite tiles for f = 1.8 GHz.

At last, an experimental-numerical procedure involving electric-field data was adopted for predicting the SAR of the sample under test. Specifically, the experimental and numerical E-fields were evaluated in correspondence of nine points positioned in the GTEM-cell test core. The obtained results were compared and a good uniformity, expressed in terms of E-field minimum to maximum ratio, was found in that restricted region. Furthermore, the linear dependence between the E-field magnitude and the input power square root was estimated to be a crucial feature for predicting with a good degree of confidence the experimental SAR in function of an assigned input power.

REFERENCES

[1] H. Frumkin, A. Jacobson, T. Gansler, M.J. Thun: *Cellular phones and risk of brain tumors,* Cancer J Clin., vol.51, pp.137-41, 2001.

[2] F. Lattarulo: *An improved model of a cell in the study of ELF electric-field interaction with living beings*, IEEE Trans. on Electrom. Compat., vol. EMC-29, pp. 64-69, Feb. 1987.

[3] M.H. Repacholi: *Health risks from the use of mobile phones*, Toxicol Lett., Vol. 120, pp. 323-31, 2001.

[4] C. Harvey, P.W. French: *Effect on protein kinase C and gene expression in a human mast cell line HMC-1, following microwave exposure*. Cell Biol. Int., vol. 23, pp. 739-48, 1999.

[5] L. Laval, Ph. Leveque, B. Jecko: *A new in vitro exposure device for the mobile frequency of 900 MHz*, Bioelectromagnetics, vol. 21, pp.255-263, 2000.

[6] J. Schuderer, T. Samaras, W. Oesch, D. Spät, N. Kuster: *High peak SAR exposure unit with tight exposure and environmental control for in vitro experiments at 1800 MHz*, IEEE Trans. on Microwave Theory and Technique, vol. 52, pp. 2057 –2066, Aug. 2004.

[7] F. Schonborn, K. Pokovic, N. Kuster: *Dosimetric analysis of the carousel setup for the exposure of rats at 1.62 GHz*, Bioelectromagnetics, vol. 25, pp.16-26, 2004.

[8] P. Galloni, G. A. Lovisolo, S. Mancini, M. Parazzini, R. Pinto, M. Piscitelli, P. Ravazzani, C. Marino: *Effects of 900 MHz electromagnetic fields exposure on cochlear cells' functionality in rats: evaluation of distortion product otoacoustic emissions*, Bioelectromagnetics, vol. 26, pp. 536-547, 2005.

[9] H. Garbe, D. Hansen: *The GTEM cell concept; applications of this new EMC test environment to radiated emission and susceptibility measurements*, Electromagnetic Compatibility, Seventh International Conference on, 28-31 Aug 1990, pp. 152 - 156.

[10] M. Zmyslony, P. Politanski, E. Rajkowska, W. Szymczak, J. Jajte: *Acute exposure to 930 MHz CW electromagnetic radiation in vitro affects reactive oxygen species level in rat lymphocytes treated by iron ions*, Bioelectromagnetics, vol. 25, pp.324-328, 2004.

[11] Z. J. Sienkiewicz, R. P. Blackwell, R.G.E. Haylock, R. D. Saunders, B. L. Cobb: *Low-level exposure to pulsed 900 MHz microwave radiation does not cause deficits in the performance of a spatial learning task in mice*, Bioelectromagnetics, vol. 21, pp. 151-158, 2000.

[12] J. Tippet, D. Chang: *Characteristic impedance of a rectangular coaxial line with offset inner conductor*, IEEE Trans. on Microwave Theory and Technique, vol. MTT-26, pp. 876 –883, Nov. 1976.

[13] R. De Leo, T. Rozzi, C. Svara, L. Zappelli: *Rigorous analysis of the GTEM cell*, IEEE Transaction on Microwave Theory and Technique, vol. MTT-39, n. 3, pp. 488-499, 1991.

[14] J. P. Kärst, C. Groh, H. Garbe: *Calculable field generation using TEM cells applied to the calibration of a novel E-Field probe*, IEEE Trans. on Electromagnetic Compatibility, vol. 44, n. 1, pp. 59-71, Feb. 2002.

[15] IEC 61000-4-3 Electromagnetic Compatibility (EMC) – Part 4-3: Testing and measurement techniques – radiated, radio-frequency, electromagnetic field immunity test, 2003.

[16] W. Mann, K. Petermann: *VCSEL-based miniaturised E-field probe with high sensitivity and optical power supply*, Electronics Letters, vol. 38, pp. 455-456, May 2002.

Giovanna Calò was born in Bari, Italy in 1976. She received the Laurea degree in Electronic Engineering and the Ph.D. degree in Electromagnetisms from the Politecnico di Bari, Italy, in 2002 and in 2006, respectively.
In 2002, she joined the Dipartimento di Elettrotecnica ed Elettronica, Politecnico di Bari, where she is currently working on scientific research projects. Her research interests concern biological effects of electromagnetic fields, dosimetry, design and characterization of GTEM cells, waveguiding devices, reverberating chambers.

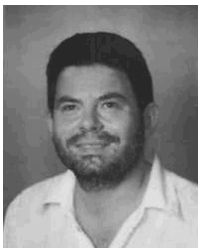

Francesco Lattarulo, 1951, was researcher in High-Voltage Engineering from 1977 to 1985; from 1985 to 1999 he was Associate Professor in Electrotechnology and since 1999 he has been full professor in Fundamentals of Electrical Engineering and Electromagnetic Compatibility. His primary interest is in some topics of applied electrostatics which include EMC and d.c. corona. Dr. Lattarulo has been appointed as a member of the AEI Special Group on EMC and a member of the CEI Technical Committee of EMC.

Vincenzo Petruzzelli was born in Bari (Italy) on 1955 and graduated in Electrical Engineering from the University of Bari on 1986. Since then he has joined the Dipartimento di Elettrotecnica ed Elettronica of Politecnico di Bari, receiving in 1992 the Ph. D. in Electronic Engineering (Electromagnetism). Currently he is Associate Professor in Electromagnetic Fields at the Dipartimento di Elettrotecnica ed Elettronica of Politecnico di Bari. Now he is engaged in theoretical and technological research on integrated optic devices, titanium diffused lithium niobate waveguides, ion-exchanged waveguides, nonlinear optics, optical fiber and on modeling of waveguiding passive and active structures. He has over 120 publications as co-author, 80 of which published on journals and international conferences, lectures and invited papers. He is involved in several national and international projects and co-operations.